Hyperpolarised ^{13}C-MRI metabolic and functional imaging: an emerging renal MR diagnostic modality

Michael Pedersen[1], Stephan Ursprung[2], Jens Dam Jensen[3], Bente Jespersen[3], Ferdia Gallagher[2], Christoffer Laustsen[4]

[1]Comparative Medicine lab, Aarhus University, Aarhus, Denmark

[2]Department of Radiology, University of Cambridge, Addenbrooke's Hospital, Cambridge, UK

[3]Department of Renal Medicine, Aarhus University Hospital, Aarhus, Denmark

[4]MR Research Centre, Department of Clinical Medicine, Aarhus University, Aarhus, Denmark

Keywords: Renal, kidney, metabolism, hyperpolarisation, MRI

Corresponding author:

Christoffer Laustsen

Aarhus University Hospital, MR Center, Palle Juul Jensens Boulevard

8200 Aarhus N

Denmark

M +45 24439141

Email: cl@clin.au.dk

This is a pre-print of an article published in "Magnetic Resonance Materials in Physics, Biology and Medicine" The final authenticated version is available online at: https://doi.org/10.1007/s10334-019-00801-y

Abstract

Magnetic Resonance Imaging (MRI) is a well-established modality for assessing renal morphology and function, as well as changes that occur during disease. However, the significant metabolic changes associated with renal disease are more challenging to assess with MRI. Hyperpolarized carbon-13 MRI is an emerging technique which provides an opportunity to probe metabolic alterations at high sensitivity by providing an increase in the signal-to-noise ratio of 20,000-fold or more. This review will highlight the current status of hyperpolarised ^{13}C-MRI and its translation into the clinic and how it compares to metabolic measurements provided by competing technologies such as Positron Emission Tomography (PET).

Introduction

The kidneys account for approximately 20% of oxygen (O_2) consumption in humans, second only to the heart (1). While renal blood flow is high, the kidneys undergo a relatively low arterio-venous oxygen extraction and are therefore particularly susceptible to hypoxic injury. Consequently, renal hypoxia plays an important role in the development and progression of both acute and chronic renal disease (1-3). This relationship is confounded by the heterogeneous nature of perfusion and O_2 consumption within the kidneys, as illustrated by the significant difference in pO_2 between the renal cortex and medulla. Furthermore, of the total renal oxygen consumption of 2.7 mmol O_2/(kg×min), about 95% of oxygen is consumed in the cortex (4). With regards to oxygen availability, it has been proposed that the renal medulla is divided into at least two distinct zones (5), where the deeper region of the medulla relies heavily on anaerobic respiration and is adapted to low pO_2 levels. Although the outer medulla is also capable of glycolysis, this well-perfused and oxygenated region undergoes aerobic metabolism. Thus, in order to maintain the tubular reabsorption of water (or medullary concentrating ability) while avoiding tubular hypoxia, the oxygen availability and blood flow to the renal medulla must be closely matched to the metabolic demands of tissue. This functional heterogeneity is maintained through cellular diversity, in which morphologically distinct cells perform specialised functions enabled by distinct enzymes (6). For example, enzymes catalysing irreversible reactions within gluconeogenesis are located predominantly in the proximal tubular cells (7), while those concerned with glucose degradation are distributed mainly in more distal segments of the nephron (8).

These intrarenal differences in metabolism and oxygen availability are important for the development of many renal diseases and imaging the spatial distribution of these changes is important for metabolic phenotyping and disease characterisation. Furthermore, measurements of these parameters could not only be used to evaluate metabolic therapies, but could also support the development of novel pharmaceutical agents specifically designed to improve the oxygen supply/demand balance or to maintain sufficient metabolism in the kidney. In this review, we outline two non-invasive diagnostic methods capable of imaging the renal metabolism, positron emission tomography (PET) and hyperpolarized magnetic resonance imaging (MRI).

Positron emission tomography (PET)

PET provides the high sensitivity and quantitative accuracy required for molecular and functional imaging. A number of PET imaging platforms are available, including PET in conjunction with

computed tomography (PET/CT) or magnetic resonance imaging (PET/MRI). Both PET/CT and PET/MRI combine the benefits of imaging tissue anatomy, function and metabolism in one study, leveraging the benefits of each modality. While PET imaging has been shown to be particularly useful in oncology, neurology and cardiology, it is not used routinely as a clinical tool in renal diseases. The majority of PET tracers are radiolabelled with either ^{18}F or ^{11}C, but other isotopes such as ^{64}Cu, ^{68}Ga, ^{89}Zr and ^{124}I are also used, particularly in research studies. ^{18}F-labeled tracers offer some key technical and procedural advantages over ^{11}C, including a longer half-life (109.6 vs 20.4 min), enabling multiple examinations in multiple patients from a single formulation and transportation to other PET facilities. ^{18}F-labeled tracers also offer an intrinsically higher image resolution due to the lower energy and shorter range of positrons in soft tissue (9). The long half-life of ^{18}F-labelled tracers restricts the possibility for retest examinations or sequential tracer examinations within the same scan session. Conversely, endogenous compounds can be radiolabelled with ^{11}C without changing their biofunctional and metabolic properties. Moreover, ^{11}C is a perfect radionuclide for labelling of small bioactive organic molecules.

An important obstacle for PET in renal examinations is the renal handling of most clinically available tracers. For example, 2-^{18}fluoro-2-deoxyglucose (^{18}F-FDG), the most widely available PET tracer and a glucose analogue (Fig 1), is avidly transported and phosphorylated in metabolically active tissues such as many tumours, but the abundance of the ^{18}F-FDG signal from urine makes any metabolic alterations present in disease states very difficult to assess in the kidney. The accumulation of ^{18}F-FDG in the urine is due to the reduced affinity of the sodium glucose cotransporter for tubular reabsorption of ^{18}F-FDG compared to glucose; unlabelled glucose is largely retained in the body by active reabsorption (10) and therefore undergoes very different renal handling. While this has limited the application of ^{18}F-FDG-PET in studies of kidney metabolism, Hato *et al.* have demonstrated an increased cortical ^{18}F-FDG uptake following the pharmacological inhibition of the gene p53 (p53 regulates genes in pathways such as oxidative respiration and glycolysis for energy generation and glucose homeostasis) (9), providing a proof of concept that PET can detect changes in cellular glucose utilisation.

^{11}C-labelled compounds have also been investigated for investigating the renal metabolism. Shreve *et al.* have recently demonstrated excellent renal imaging obtained by PET using ^{11}C-acetate (11), and this approach was suggested as a biomarker for renal oxidative metabolism via the tricarboxylic acid cycle (12). Recently, Splan *et al.* showed that ^{11}C-choline successfully reveals the renal tubular function (13). $H_2{}^{15}O$ has been used as a non-invasive clinical tracer to image tissue blood flow (Fig

2). $H_2{}^{15}O$, is a particularly suitable renal perfusion biomarker because it is diffusible and is neither extracted nor metabolised in the kidney and has a short half-life (2 min), allowing multiple examinations during the same scan session (14) (Fig 1).

Hyperpolarised ^{13}C-MRI

Hyperpolarised ^{13}C-MRI is an emerging molecular imaging method that allows rapid, non-invasive and pathway-specific investigation of dynamic, metabolic and physiologic processes, previously not possible with imaging. Hyperpolarised ^{13}C-labelled agents enhance the signal-to-noise ratio *in vivo* more than 20,000-fold compared to conventional, non-hyperpolarised ^{13}C-MRI and is capable of capturing perfusion, uptake and subsequent metabolic conversion of tracers and could have great potential in studying metabolic renal disorders (15-18) (Fig 3).

Hyperpolarised ^{13}C-based bioprobes enable direct quantification of tracer concentrations similar to tracers in PET scans, where the tracer itself emits the signal rather than modulating the surrounding tissue, as seen in standard contrast-enhanced MRI. Hyperpolarised MRI utilises molecules labelled with ^{13}C (or other MR-active nuclei), which undergo dynamic nuclear polarisation (DNP) and rapid dissolution to create an injectable solution (19-21). Following injection of a hyperpolarised substrate, the enzymatic conversion of the injected substrate can be detected. DNP relies on the principle of transferring a higher polarisation or energy level from one spin (typically electrons) to another nuclear spin (typically ^{13}C) (20, 21). This process is accomplished by irradiating electrons with a microwave frequency that matches the resonance frequency of the combined system of electron and ^{13}C-nuclear spins. In order to achieve maximum polarisation of the target nuclear spin, the spins system is cooled to <1 K (-272 °C). The process to polarise ^{13}C-containing molecules takes approximately 2 h, typically using a magnetic field strength of 5 T. After the sample has polarised, it is rapidly heated and administered by venous bolus injection to the subject within the MRI system, similar to conventional contrast-agent administration (21).

Pioneering work by Golman *et al.* showed the potential of hyperpolarised MRI in renal diagnostics (22), demonstrating catheter tracking, renal angiography and perfusion assessment (23). Furthermore, the technique holds the potential for *in situ* tracing of metabolic conversion of injected metabolic bioprobes to their product metabolites in renal tissue (24, 25). Following these discoveries, several hyperpolarised substances have been proposed as new potential diagnostic markers in renal disease. The most well-established substance is hyperpolarised [1-^{13}C]pyruvate, the first hyperpolarised bioprobe to be assessed in humans (16, 18).

Imaging glycolysis with [1-^{13}C]pyruvate

Following intravenous injection of hyperpolarised [1-^{13}C]pyruvate, the molecule is distributed in the blood and transported intracellularly, particularly in well-vascularised and perfused organs such as the kidneys (17, 18). Pyruvate, the end-product of glycolysis, undergoes oxidation in the mitochondria by entering the tricarboxylic acid (TCA) cycle via pyruvate dehydrogenase, transamination in the cytosol via alanine transaminase (ALT) forming alanine or, under anaerobic conditions, conversion to lactate via lactate dehydrogenase (LDH) (Fig 4). The injected pyruvate and its metabolism can be detected by the chemical shift of the product and substrates on MR spectroscopy i.e. the conversion of [1-^{13}C]pyruvate (detected at 170.4 ppm) to [1-^{13}C]lactate (183 ppm), [1-^{13}C]alanine (176 ppm) and $^{13}CO_2$ (125 ppm)/$H^{13}CO^-_3$ (160 ppm). The ability to investigate multiple metabolic pathways (aerobic and anaerobic) in one single examination within a couple of minutes offers a new approach to imaging haemodynamics and metabolism simultaneously using MRI (23, 26-37). By labelling the molecular C2 position instead of the C1 position of pyruvate molecules, the ^{13}C label can be detected within the TCA cycle (38).

In a rat model of streptozotocin-induced type-1 diabetes, hyperpolarised [1-^{13}C]pyruvate and BOLD ^{1}H-MRI were employed to investigate changes in renal physiology *in vivo* (39). In that study, diabetic kidneys showed an increased metabolic flux in anaerobic pathways, such as an increased lactate/pyruvate ratio compared to healthy kidneys, whereas the bicarbonate/pyruvate ratio, a surrogate marker for aerobic metabolism, remained unchanged. This oxygen metabolic reprogramming was paralleled by a reduced intrarenal oxygen availability and/or increased consumption identified by oxygen-dependent hyperpolarised ^{13}C-urea T2-weighted imaging (40) and by BOLD MRI (39). In another study, streptozotocin-induced diabetic rats were exposed to alternating oxygen concentration in the inspired air, which altered renal tissue oxygenation (41). The renal metabolic effects were studied using hyperpolarised [1-^{13}C]pyruvate MRI and BOLD ^{1}H-MRI, demonstrating that the reduced oxygen availability in the diabetic kidney altered energy metabolism via increased lactate and alanine formation, while the bicarbonate flux remained unchanged. Thus, these results support the view that the increased prevalence and severity of nephropathy in patients with diabetes at high altitudes may originate from increased oxygen sensitivity (41), and that hyperpolarised MRI shows promise in the diagnosis and monitoring of early renal changes associated with diabetes. Importantly, lactate production not only correlates with the severity of renal dysfunction and its progression, it also represents a novel measure of therapeutic response. Similar to

hypoxia, glucose-lowering drugs such as insulin and metformin treatment in diabetic rats have been shown to increase lactate production while LDH inhibitor therapies, such as hyperbaric oxygen therapy and antioxidant treatment, have shown to reduce renal lactate production (27, 31, 37, 42-44). The kidney not only consumes glucose, but it may also generate glucose as part of gluconeogenesis. In the renal cortex, gluconeogenic enzymes (phosphoenolpyruvate carboxykinase (PEPCK), fructose-1,6-bisphosphatase glucose-6-phosphatase) synthesise glucose-6-phosphate from precursors such as lactate, glutamine, glycerol and alanine (37, 44). Alterations in the renal redox balance imposed by inhibition of the gluconeogenic pathway via 5' adenosine monophosphate-activated protein kinase have been investigated using hyperpolarised [1-^{13}C]pyruvate (31, 45). However, more specific biomarkers such as [1-^{13}C]dehydroascorbate (DHA), [2-^{13}C]dihydroxyacetone, ^{13}C-glycerate or [1-^{13}C]alanine could provide additional insight, particularly in pre-clinical research (46-49).

Many mutations commonly observed in renal cell carcinoma (RCC) result in changes in the cellular energy metabolism (50). Additionally, metabolic alterations and increased concentrations of oncometabolites, such as succinate and fumarate, have increasingly recognised roles in tumorigenesis (51). Hyperpolarised [1-^{13}C]pyruvate MRI can be used to investigate altered tumour energy metabolism, where an increased pyruvate-to-lactate ratio is associated with malignancy and tumour aggressiveness in *in vitro* models of RCC (52, 53). In perspective, this MRI technique could play a role in early detection of treatment response in patients undergoing systemic anticancer therapy to ensure treatment efficacy and limit side-effects. For example, metabolic response to mTOR (mechanistic target of rapamycin) inhibition, a therapeutic target in RCC, can be observed as early as 24 hours after the initiation of treatment in a murine model (52). Initial patient data confirm that hyperpolarised imaging is feasible in patients with RCC and highlight the need for further clinical research to define the future role of this modality in uro-oncological imaging (54).

Hyperpolarised [1-^{13}C]pyruvate has also shown promising results in unilateral ureteral obstruction (26), acute kidney injury (both ischaemia/reperfusion and toxin-induced), as well as acute tubular necrosis (36, 55, 56). Taken together, these findings support a potential clinical use of hyperpolarised [1-^{13}C]pyruvate, although only few reports have investigated renal dysfunction in humans or animal models of renal disease (24, 29, 54).

Emerging clinical biomarkers

Clatworthy *et al.* have shown that [1-^{13}C]pyruvate metabolism was unaltered in a model of acute tubular necrosis while [1,4-$^{13}C_2$]fumarate revealed early tubular necrosis through an enzymatic

conversion of fumarate to malate catalysed by the enzyme fumarase. As fumarate is transported slowly into viable cells, its physiological conversion to malate is minimal and the detection of malate signal on MRI is associated with cell death in early tubular necrosis (56) and ischaemia/reperfusion injury (57). Another emerging hyperpolarised compound in renal MRI diagnostics is acetate, which is rapidly metabolised into acetylcarnitine in mammalian cells. Koellisch *et al.* demonstrated that conversion of ^{13}C-acetate to ^{13}C-acetylcarnitine is detectable in the kidney with an advanced MRI acquisition strategy, although they showed no differences between diabetic and healthy kidneys (58). By repurposing a kinetic analysis approach developed for ^{11}C-acetate PET, it is possible to map the metabolic clearance rate of ^{13}C-acetate, similar to that reported in ^{11}C-acetate PET studies (59). Keshari *et al.* have shown increased oxidative stress in diabetic mouse kidneys using the novel redox sensor, hyperpolarised [1-^{13}C]DHA (48). Interestingly, that study highlighted the potential of investigating oxidative stress modulation, and the authors suggested that hyperpolarised [1-^{13}C]DHA may potentially enhance the prediction and early detection of diabetic nephropathy and provide companion biomarkers that can better inform about the response to new therapies targeting oxidative stress in patients. An alternative approach for assessing the intrarenal redox state has recently been demonstrated by Von Morze *et al.* (60) using ^{13}C-acetoacetate. ^{13}C-acetoacetate to ^{13}C-β-hydroxybutyrate conversion is directly linked to the mitochondrial redox state.

The intrarenal osmolality-gradient is driven by the active transport of ions and water and is closely linked to renal function. A particularly appealing emerging clinical probe for renal investigations is the osmolite ^{13}C-urea, which has been demonstrated in pre-clinical models to allow assessment of pathological changes in kidney diseases (28, 32, 61), as well as functional states such as the difference between hydration and diuresis (35, 62, 63). By utilising [^{13}C,^{15}N]urea as a probe, it is possible to increase the longitudinal and transverse relaxation times (T1 and T2 relaxation) of the hyperpolarised state, and thus, [^{13}C,^{15}N]urea could potentially be used in future clinical studies, thereby extending the imaging window (33). As urea shows many biochemical characteristics similar to water, urea relaxation properties might be used to differentiate physiological and diseased states similar to conventional functional proton MRI methods such as BOLD (64, 65). Furthermore, rodent data suggests that besides perfusion, the [^{13}C,^{15}N]urea first-pass uptake-curve may reflect renal GFR (66), and could be used instead of gadolinium-containing contrast-agents (67-69) extending what is possible with non-contrast enhanced methods such as arterial spin labelling. Hyperpolarised H_2O could provide haemodynamic information inside the kidneys in a way similar to $H_2{}^{15}O$ PET, with the

advantage of providing angiographic imaging owing to the increased temporal resolution of MRI compared to PET (70).

Discussion

The metabolic status of the kidney may indicate susceptibility to injury and is considered a measure of progression in many renal disease processes. However, non-invasive clinical methods to image kidney metabolism are lacking. In this review, we have addressed methods for imaging oxygenation and metabolism in the kidney. The complex pathophysiology of renal disease is tightly connected with metabolic alterations. Despite developments in the mechanistic understanding of renal diseases, the potential causality between metabolic changes and disease development is poorly understood. Overt diabetic nephropathy, for example, is characterised by proteinuria, a decline in renal function, decreasing GFR, glomerulosclerosis and interstitial fibrosis (71); however, accurate and non-invasive biomarkers of disease progression are needed to monitor the multifactorial progression associated with the metabolic, functional and haemodynamic status in this and other renal diseases (72).

Hyperpolarised MRI is promising but still lacks largescale and widespread validation and implementation in clinical kidney examinations. Like the sterile environment in every PET facility, production and use of hyperpolarised nuclei are subject to production criteria, ensuring a safe and injectable product. The tolerability of the intravenous injected supraphysiological concentration of (0.43ml/kg 250 mM) pyruvate has been shown to be high in humans (18, 54, 73-77). [1-^{13}C]pyruvate is the first hyperpolarised bioprobe available for human use, but other candidate clinical molecules are being developed, including [2-^{13}C]pyruvate, [1,4-^{13}C]fumarate, ^{13}C-urea and [1-^{13}C]lactate.

In conclusion, MRI is a powerful non-invasive tool for renal imaging, where functional and morphological information can aid both researchers and clinicians. An important advantage of MRI is the lack of ionising radiation, allowing repeated measurements over the course of a disease. Hyperpolarised MRI increases the sensitivity of MRI by several orders of magnitude and has shown great promise as a diagnostic modality for precision medicine in kidneys.

Table 1: Metabolic and functional imaging biomarkers for renal imaging.

Compound	Modality	Pathway/function	Strength	Weakness	References
2-^{18}F-2-Deoxyglucose (FDG)	PET	Glucose uptake	Sensitive; Long half-life	Renal accumulation; Long half-life	(78)
^{11}C-acetate	PET	Tricarboxylic acid cycle flux	Metabolically active	Relatively long half-life	(12)
$H_2{}^{15}0$	PET	Perfusion	Short half-life	Short half-life	(79)
[1-^{13}C]pyruvate	HP	Glycolysis, tricarboxylic acid cycle flux	High Polarisation; Central metabolic position	Supraphysiological concentrations	(24)
[2-^{13}C]pyruvate	HP	Glycolysis, tricarboxylic acid cycle flux	High Polarisation; Central metabolic position.	Supraphysiological concentrations; shorter T1 relaxation compared to [1-^{13}C]pyruvate	(38, 80)
[1-^{13}C]lactate	HP	Glycolysis, tricarboxylic acid cycle flux	Physiological concentrations; High Polarisation; unique metabolic position.	Low intracellular pyruvate pool.	(37)
^{13}C-urea or [^{13}C,$^{15}N_2$]urea	HP	Perfusion, function	High polarisation and long lived (^{15}N)	^{14}N is a quadrupolar spin.	(35, 62)
[1,4-^{13}C]fumarate	HP	Cell death	Almost binary cell death marker	Splitting of the peaks.	(35) (57)
^{13}C-Acetate	HP	Perfusion, tricarboxylic acid cycle flux	Endogenous	Overlapping peaks at 3T	(59)
α-trideuteromethyl-[^{15}N]glutamine	HP	Perfusion	Very long lived	Relative low SNR on ^{15}N	(81, 82)
^{13}C-acetoacetate	HP	Mitochondrial redox state	Specific mitochondrial redox marker	Relative low polarisation	(60)
$^{1}H_2O$	HP	Angiogram/Perfusion	High SNR; no need for special coils	Very short relaxation time	(70)
HP001	HP	Angiogram/Perfusion	Long lived and non-metabolic	Special synthesis, artificial molecule	(83)
[1-^{13}C]dehydroascorbate	HP	Redox state	Specific redox marker	Supraphysiological concentrations	(47)

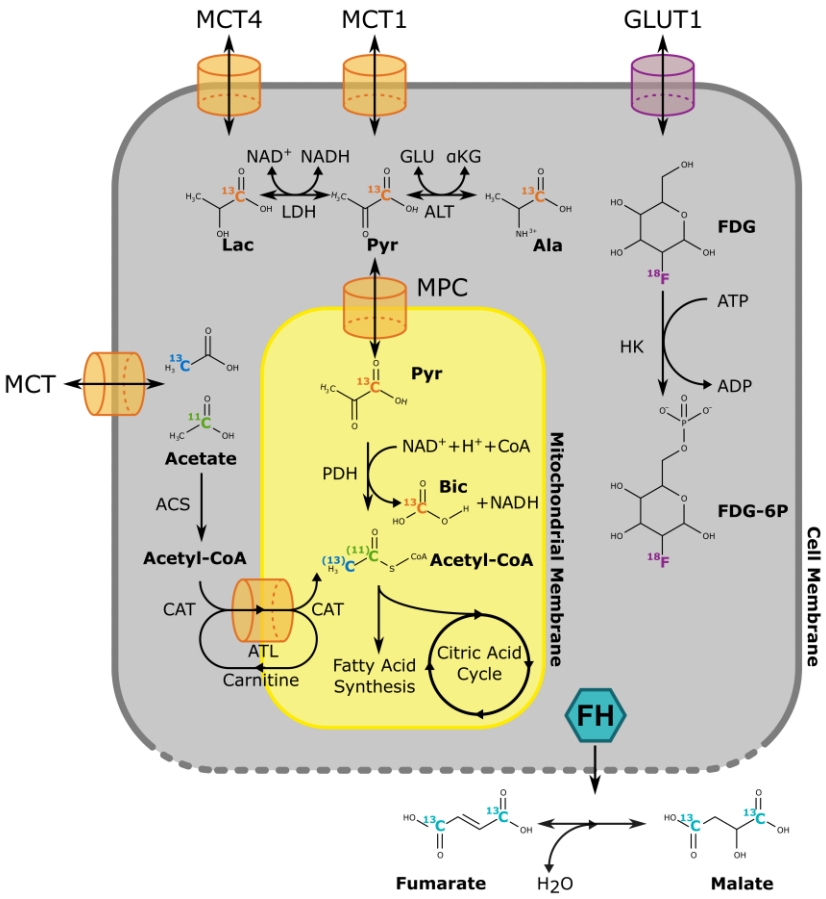

Fig 1. Metabolism of tracers used in renal imaging. Pyruvate is taken up into the cell through the monocarboxylate transporter 1 (MCT1) and rapidly metabolised in the cytosol to lactate and alanine. Following mitochondrial uptake through the mitochondrial pyruvate carrier (MPC), pyruvate dehydrogenase (PDH) catalysis the formation of Acetyl-CoA and transfer of the ^{13}C-label to bicarbonate. Downstream metabolites of [1-^{13}C]pyruvate can be spectrally resolved, which stands in contrast with FDG. After uptake through the GLUT1 transporter, FDG undergoes hexokinase (HK) mediated phosphorylation and FDG-6P is fixated in the cell. MR-active [2-^{13}C]acetate and radioactive [1-^{11}C]acetate are rapidly metabolised to Acetyl-CoA and taken up into the mitochondria where they enter the citric acid cycle or fatty acid synthesis. Fumarate hydratase (FH) is released from cells undergoing necrosis as a result of increased membrane permeability, resulting in rapid conversion of fumarate to malate.

ACS: Acetyl-CoA synthetase, Ala: Alanine, ALT: Alanine Aminotransferase, ATL: Acetylcarnitine Translocase, Bic: Bicarbonate, CAT: Carnitine O-Acetyltransferase, CoA: Coenzyme A, FDG:

Fluorodeoxyglucose, FDG-6P: Flurodeoxyglucose 6-phosphate, FH: Fumarate Hydratase, GLUT: Glucose Transporter, HK: Hexokinase, Lac: Lactate, LDH: Lactate Dehydrogenase, MCT: Monocarboxylate Transporter, MPC: Mitochondrial Pyruvate Carrier, Pyr: Pyruvate.

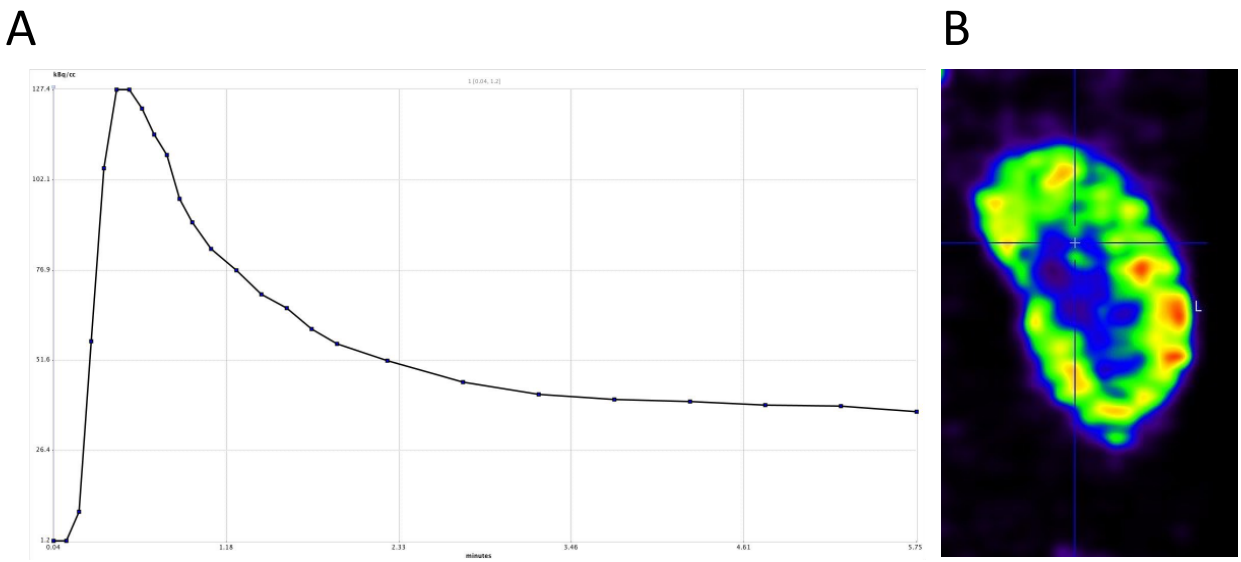

Fig 2. Renal blood perfusion measurement by PET using $H_2{}^{15}O$. The dynamic uptake of the radioactive tracer (A), and accumulated signal intensity, a surrogate marker of renal blood perfusion.

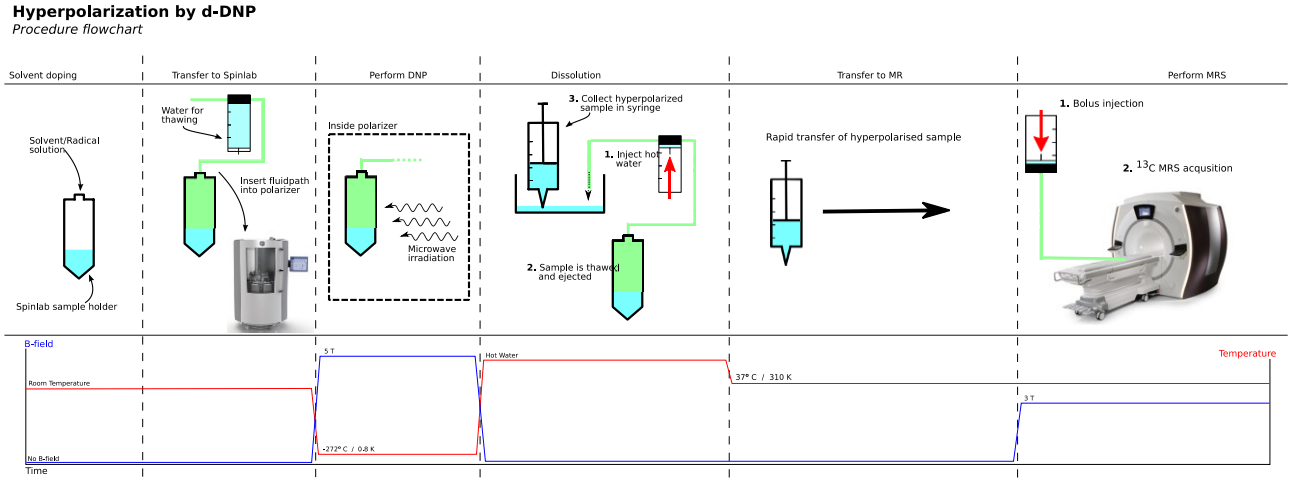

Fig 3. A hyperpolariser can make use of the dynamic nuclear polarisation (DNP) methodology, which is able to transfer excess heat or energy from the electron spin to the nuclear spin of choice (for example ^{13}C). This energy transfer is achieved by freezing the sample (-272 ºC), in a strong magnet field (usually 3-5 T), and by irradiating the sample with microwaves with a specific frequency determined by the magnetic field and the nuclear spins of interested. The sample are finally transferred by rapidly thawing the polarised sample using heated water.

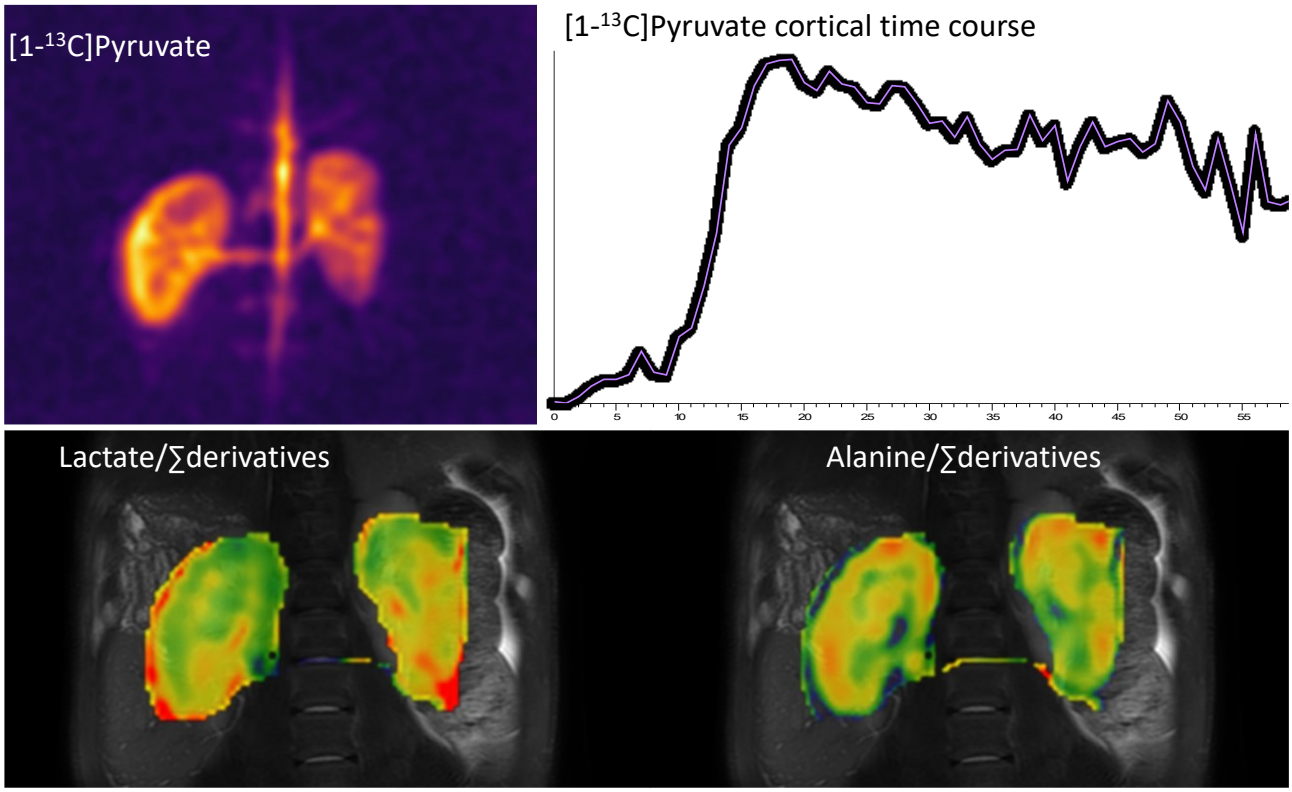

Fig 4: (Top left) single time point [1-^{13}C]pyruvate image showing the pyruvate distribution 20 s after injection. (Top right) a cortical ROI signal change for 60 s. (Lower left-right) [1-^{13}C]lactate and [1-^{13}C]alanine distribution normalised to the generated metabolites (from the injected [1-^{13}C]pyruvate), showing a heterogeneous distribution.

Compliance with Ethical Standards

Funding: This study was funded by Aarhus University Research Foundation and Karen Elise Jensen Foundation. Conflict of Interest: CL, SU, MP, BJ, JDJ, FG declares no conflict of interest. Ethical approval: All applicable international, national, and/or institutional guidelines for the care and use of animals were followed.

References

1. Haase VH. Mechanisms of hypoxia responses in renal tissue. Journal of the American Society of Nephrology : JASN. 2013;24(4):537-41.
2. Fiorentino M, Grandaliano G, Gesualdo L, Castellano G. Acute Kidney Injury to Chronic Kidney Disease Transition. Contributions to nephrology. 2018;193:45-54.
3. Ow CPC, Ngo JP, Ullah MM, Hilliard LM, Evans RG. Renal hypoxia in kidney disease: Cause or consequence? Acta physiologica (Oxford, England). 2018;222(4):e12999.
4. Singh P, Ricksten SE, Bragadottir G, Redfors B, Nordquist L. Renal oxygenation and haemodynamics in acute kidney injury and chronic kidney disease. Clinical and experimental pharmacology & physiology. 2013;40(2):138-47.
5. O'Connor PM. Renal oxygen delivery: matching delivery to metabolic demand. Clinical and experimental pharmacology & physiology. 2006;33(10):961-7.
6. Lawrence GM, Jepson MA, Trayer IP, Walker DG. The compartmentation of glycolytic and gluconeogenic enzymes in rat kidney and liver and its significance to renal and hepatic metabolism. The Histochemical journal. 1986;18(1):45-53.
7. Burch HB, Narins RG, Chu C, Fagioli S, Choi S, McCarthy W, et al. Distribution along the rat nephron of three enzymes of gluconeogenesis in acidosis and starvation. The American journal of physiology. 1978;235(3):F246-53.
8. Schmidt U, Marosvari I, Dubach UC. Renal metabolism of glucose: anatomical sites of hexokinase activity in the rat nephron. FEBS letters. 1975;53(1):26-8.
9. Tai YC, Laforest R. Instrumentation aspects of animal PET. Annual review of biomedical engineering. 2005;7:255-85.
10. Qiao H, Bai J, Chen Y, Tian J. Kidney modelling for FDG excretion with PET. Int J Biomed Imaging. 2007;2007:63234-.
11. Shreve P, Chiao PC, Humes HD, Schwaiger M, Gross MD. Carbon-11-acetate PET imaging in renal disease. Journal of nuclear medicine : official publication, Society of Nuclear Medicine. 1995;36(9):1595-601.
12. Juillard L, Lemoine S, Janier MF, Barthez PY, Bonnefoi F, Laville M. Validation of renal oxidative metabolism measurement by positron-emission tomography. Hypertension (Dallas, Tex : 1979). 2007;50(1):242-7.
13. Splan A, Borofka M, Casper K, Fischer N, Gunderson T, Rule A, et al. 11C-Choline PET for Evaluation of Renal Tubular Function. Journal of Nuclear Medicine. 2018;59(supplement 1):2147.
14. Juillard L, Janier MF, Fouque D, Lionnet M, Le Bars D, Cinotti L, et al. Renal blood flow measurement by positron emission tomography using ¹⁵O-labeled water. Kidney international. 2000;57(6):2511-8.
15. Rider OJ, Tyler DJ. Clinical implications of cardiac hyperpolarized magnetic resonance imaging. Journal of cardiovascular magnetic resonance : official journal of the Society for Cardiovascular Magnetic Resonance. 2013;15:93.
16. Kurhanewicz J, Vigneron DB, Brindle K, Chekmenev EY, Comment A, Cunningham CH, et al. Analysis of cancer metabolism by imaging hyperpolarized nuclei: prospects for translation to clinical research. Neoplasia (New York, NY). 2011;13(2):81-97.
17. Laustsen C. Hyperpolarized Renal Magnetic Resonance Imaging: Potential and Pitfalls. Frontiers in physiology. 2016;7:72.

18. Kurhanewicz J, Vigneron DB, Ardenkjaer-Larsen JH, Bankson JA, Brindle K, Cunningham CH, et al. Hyperpolarized (13)C MRI: Path to Clinical Translation in Oncology. Neoplasia (New York, NY). 2018;21(1):1-16.
19. Ardenkjaer-Larsen JH, Bowen S, Petersen JR, Rybalko O, Vinding MS, Ullisch M, et al. Cryogen-free dissolution dynamic nuclear polarization polarizer operating at 3.35 T, 6.70 T, and 10.1 T. Magn Reson Med. 2018.
20. Ardenkjaer-Larsen JH, Fridlund B, Gram A, Hansson G, Hansson L, Lerche MH, et al. Increase in signal-to-noise ratio of > 10,000 times in liquid-state NMR. Proceedings of the National Academy of Sciences of the United States of America. 2003;100(18):10158-63.
21. Ardenkjaer-Larsen JH, Leach AM, Clarke N, Urbahn J, Anderson D, Skloss TW. Dynamic nuclear polarization polarizer for sterile use intent. NMR in biomedicine. 2011;24(8):927-32.
22. Golman K, Axelsson O, Jóhannesson H, Månsson S, Olofsson C, Petersson JS. Parahydrogen-induced polarization in imaging: Subsecond 13C angiography. Magnetic Resonance in Medicine. 2001;46(1):1-5.
23. Johansson E, Olsson LE, Månsson S, Petersson JS, Golman K, Ståhlberg F, et al. Perfusion assessment with bolus differentiation: A technique applicable to hyperpolarized tracers. Magnetic Resonance in Medicine. 2004;52(5):1043-51.
24. Fast multiecho balanced SSFP metabolite mapping of 1H and hyperpolarized 13C compounds, (2009).
25. Golman K, Petersson JS. Metabolic Imaging and Other Applications of Hyperpolarized ¹³C¹. Academic Radiology. 2006;13(8):932-42.
26. Niles DJ, Gordon JW, Huang G, Reese S, Adamson EB, Djamali A, et al. Evaluation of renal metabolic response to partial ureteral obstruction with hyperpolarized (13) C MRI. NMR in biomedicine. 2018;31(1).
27. Laustsen C, Lipso K, Ostergaard JA, Norregaard R, Flyvbjerg A, Pedersen M, et al. Insufficient insulin administration to diabetic rats increases substrate utilization and maintains lactate production in the kidney. Physiological reports. 2014;2(12).
28. Bertelsen LB, Nielsen PM, Qi H, Norlinger TS, Zhang X, Stodkilde-Jorgensen H, et al. Diabetes induced renal urea transport alterations assessed with 3D hyperpolarized 13 C,15 N-Urea. Magn Reson Med. 2016.
29. Laustsen C, Hansen ES, Kjaergaard U, Bertelsen LB, Ringgaard S, Stodkilde-Jorgensen H. Acute porcine renal metabolic effect of endogastric soft drink administration assessed with hyperpolarized [1-13c]pyruvate. Magn Reson Med. 2015.
30. Qi H, Mariager CO, Lindhardt J, Nielsen PM, Stodkilde-Jorgensen H, Laustsen C. Effects of anesthesia on renal function and metabolism in rats assessed by hyperpolarized MRI. Magn Reson Med. 2018;80(5):2073-80.
31. Qi H, Nielsen PM, Schroeder M, Bertelsen LB, Palm F, Laustsen C. Acute renal metabolic effect of metformin assessed with hyperpolarised MRI in rats. Diabetologia. 2018;61(2):445-54.
32. Qi H, Norlinger TS, Nielsen PM, Bertelsen LB, Mikkelsen E, Xu Y, et al. Early diabetic kidney maintains the corticomedullary urea and sodium gradient. Physiological reports. 2016;4(5).
33. Reed GD, von Morze C, Bok R, Koelsch BL, Van Criekinge M, Smith KJ, et al. High Resolution <formula formulatype="inline"> <img src="/images/tex/18978.gif" alt="^{13}"> </formula>C MRI With Hyperpolarized Urea: In Vivo <formula formulatype="inline"> <img src="/images/tex/635.gif" alt="T_{2}"> </formula> Mapping and <formula

formulatype="inline"> <img src="/images/tex/21386.gif" alt="^{15}"> </formula>N Labeling Effects. Medical Imaging, IEEE Transactions on. 2014;33(2):362-71.
34. Reed GD, von Morze C, Verkman AS, Koelsch BL, Chaumeil MM, Lustig M, et al. Imaging Renal Urea Handling in Rats at Millimeter Resolution using Hyperpolarized Magnetic Resonance Relaxometry. ArXiv e-prints [Internet]. 2015 October 1, 2015; 1511:[200 p.]. Available from: http://adsabs.harvard.edu/abs/2015arXiv151100200R.
35. von Morze C, Bok RA, Sands JM, Kurhanewicz J, Vigneron DB. Monitoring urea transport in rat kidney in vivo using hyperpolarized 13C magnetic resonance imaging. American Journal of Physiology - Renal Physiology. 2012.
36. Nielsen PM, Laustsen C, Bertelsen LB, Qi H, Mikkelsen E, Kristensen ML, et al. In situ lactate dehydrogenase activity: a novel renal cortical imaging biomarker of tubular injury? American journal of physiology Renal physiology. 2017;312(3):F465-f73.
37. von Morze C, Chang G-Y, Larson PEZ, Shang H, Allu PKR, Bok RA, et al. Detection of localized changes in the metabolism of hyperpolarized gluconeogenic precursors 13C-lactate and 13C-pyruvate in kidney and liver. Magnetic Resonance in Medicine. 2017;77(4):1429-37.
38. Hu S, Yoshihara HAI, Bok R, Zhou J, Zhu M, Kurhanewicz J, et al. Use of hyperpolarized [1-13C]pyruvate and [2-13C]pyruvate to probe the effects of the anticancer agent dichloroacetate on mitochondrial metabolism in vivo in the normal rat. Magnetic resonance imaging. 2012;30(10):1367-72.
39. Laustsen C, Østergaard JA, Lauritzen MH, Nørregaard R, Bowen S, Søgaard LV, et al. Assessment of early diabetic renal changes with hyperpolarized [1-13C]pyruvate. Diabetes/Metabolism Research and Reviews. 2013;29(2):125-9.
40. Laustsen C, Stokholm Norlinger T, Christoffer Hansen D, Qi H, Mose Nielsen P, Bonde Bertelsen L, et al. Hyperpolarized C urea relaxation mechanism reveals renal changes in diabetic nephropathy. Magn Reson Med. 2015.
41. Laustsen C, Lycke S, Palm F, Ostergaard JA, Bibby BM, Norregaard R, et al. High altitude may alter oxygen availability and renal metabolism in diabetics as measured by hyperpolarized [lsqb]1-13C[rsqb]pyruvate magnetic resonance imaging. Kidney international. 2013.
42. Norlinger TS, Nielsen PM, Qi H, Mikkelsen E, Hansen K, Schmidt NH, et al. Hyperbaric oxygen therapy reduces renal lactate production. Physiological reports. 2017;5(6).
43. Laustsen C, Nielsen PM, Norlinger TS, Qi H, Pedersen UK, Bertelsen LB, et al. Antioxidant treatment attenuates lactate production in diabetic nephropathy. American journal of physiology Renal physiology. 2017;312(1):F192-f9.
44. Morze Cv, Allu PKR, Chang GY, Marco-Rius I, Milshteyn E, Wang ZJ, et al. Non-invasive detection of divergent metabolic signals in insulin deficiency vs. insulin resistance in vivo. Scientific reports. 2018;8(1):2088.
45. Lewis AJ, Miller JJ, McCallum C, Rider OJ, Neubauer S, Heather LC, et al. Assessment of Metformin-Induced Changes in Cardiac and Hepatic Redox State Using Hyperpolarized[1-13C]Pyruvate. Diabetes. 2016;65(12):3544-51.
46. Park JM, Wu M, Datta K, Liu SC, Castillo A, Lough H, et al. Hyperpolarized Sodium [1-(13)C]-Glycerate as a Probe for Assessing Glycolysis In Vivo. Journal of the American Chemical Society. 2017;139(19):6629-34.
47. Park JM, Khemtong C, Liu SC, Hurd RE, Spielman DM. In vivo assessment of intracellular redox state in rat liver using hyperpolarized [1-(13) C]Alanine. Magn Reson Med. 2017;77(5):1741-8.

48. Keshari KR, Wilson DM, Sai V, Bok R, Jen KY, Larson P, et al. Noninvasive in vivo imaging of diabetes-induced renal oxidative stress and response to therapy using hyperpolarized 13C dehydroascorbate magnetic resonance. Diabetes. 2015;64(2):344-52.
49. Marco-Rius I, von Morze C, Sriram R, Cao P, Chang GY, Milshteyn E, et al. Monitoring acute metabolic changes in the liver and kidneys induced by fructose and glucose using hyperpolarized [2-(13) C]dihydroxyacetone. Magn Reson Med. 2017;77(1):65-73.
50. Linehan WM, Srinivasan R, Schmidt LS. The genetic basis of kidney cancer: a metabolic disease. Nature reviews Urology. 2010;7(5):277-85.
51. Sciacovelli M, Frezza C. Oncometabolites: Unconventional triggers of oncogenic signalling cascades. Free radical biology & medicine. 2016;100:175-81.
52. Dong Y, Eskandari R, Ray C, Granlund KL, Santos-Cunha LD, Miloushev VZ, et al. Hyperpolarized MRI Visualizes Warburg Effects and Predicts Treatment Response to mTOR Inhibitors in Patient-Derived ccRCC Xenograft Models. Cancer research. 2019;79(1):242-50.
53. Sriram R, Gordon J, Baligand C, Ahamed F, Delos Santos J, Qin H, et al. Non-Invasive Assessment of Lactate Production and Compartmentalization in Renal Cell Carcinomas Using Hyperpolarized (13)C Pyruvate MRI. Cancers. 2018;10(9).
54. Tran M, Latifoltojar A, Neves JB, Papoutsaki M-V, Gong F, Comment A, et al. First-in-human in vivo non-invasive assessment of intra-tumoral metabolic heterogeneity in renal cell carcinoma. BJR|case reports. 2019:20190003.
55. Baligand C, Qin H, True-Yasaki A, Gordon JW, von Morze C, Santos JD, et al. Hyperpolarized (13) C magnetic resonance evaluation of renal ischemia reperfusion injury in a murine model. NMR in biomedicine. 2017;30(10).
56. Clatworthy MR, Kettunen MI, Hu D-E, Mathews RJ, Witney TH, Kennedy BWC, et al. Magnetic resonance imaging with hyperpolarized [1,4-13C2]fumarate allows detection of early renal acute tubular necrosis. Proceedings of the National Academy of Sciences. 2012;109(33):13374-9.
57. Nielsen PM, Eldirdiri A, Bertelsen LB, Jorgensen HS, Ardenkjaer-Larsen JH, Laustsen C. Fumarase activity: an in vivo and in vitro biomarker for acute kidney injury. Scientific reports. 2017;7:40812.
58. Koellisch U, Laustsen C, Norlinger TS, Ostergaard JA, Flyvbjerg A, Gringeri CV, et al. Investigation of metabolic changes in STZ-induced diabetic rats with hyperpolarized [1-13C]acetate. Physiological reports. 2015;3(8).
59. Mikkelsen EFR, Mariager CO, Norlinger T, Qi H, Schulte RF, Jakobsen S, et al. Hyperpolarized [1-(13)C]-acetate Renal Metabolic Clearance Rate Mapping. Scientific reports. 2017;7(1):16002.
60. von Morze C, Ohliger MA, Marco-Rius I, Wilson DM, Flavell RR, Pearce D, et al. Direct assessment of renal mitochondrial redox state using hyperpolarized (13) C-acetoacetate. Magn Reson Med. 2018;79(4):1862-9.
61. Nielsen PM, Szocska Hansen ES, Norlinger TS, Norregaard R, Bonde Bertelsen L, Stodkilde Jorgensen H, et al. Renal ischemia and reperfusion assessment with three-dimensional hyperpolarized (13) C,(15) N2-urea. Magn Reson Med. 2016;76(5):1524-30.
62. Hansen ES, Stewart NJ, Wild JM, Stodkilde-Jorgensen H, Laustsen C. Hyperpolarized (13) C,(15) N2 -Urea MRI for assessment of the urea gradient in the porcine kidney. Magn Reson Med. 2016;76(6):1895-9.
63. Qi H, Mariager CO, Nielsen PM, Schroeder M, Lindhardt J, Norregaard R, et al. Glucagon infusion alters the hyperpolarized (13) C-urea renal hemodynamic signature. NMR in biomedicine. 2019;32(1):e4028.

64. Laustsen C, Stokholm Norlinger T, Christoffer Hansen D, Qi H, Mose Nielsen P, Bonde Bertelsen L, et al. Hyperpolarized 13C urea relaxation mechanism reveals renal changes in diabetic nephropathy. Magn Reson Med. 2016;75(2):515-8.
65. Mariager CO, Nielsen PM, Qi H, Ringgaard S, Laustsen C. Hyperpolarized (13) C,(15) N2 -urea T2 relaxation changes in acute kidney injury. Magn Reson Med. 2018;80(2):696-702.
66. Ostergaard Mariager C, Nielsen PM, Qi H, Schroeder M, Bertelsen LB, Laustsen C. Can Hyperpolarized (13)C-Urea be Used to Assess Glomerular Filtration Rate? A Retrospective Study. Tomography (Ann Arbor, Mich). 2017;3(3):146-52.
67. Zöllner FG, Zimmer F, Klotz S, Hoeger S, Schad LR. Renal perfusion in acute kidney injury with DCE-MRI: Deconvolution analysis versus two-compartment filtration model. Magnetic Resonance Imaging. 2014;32(6):781-5.
68. Zimmer F, Zöllner FG, Hoeger S, Klotz S, Tsagogiorgas C, Krämer BK, et al. Quantitative Renal Perfusion Measurements in a Rat Model of Acute Kidney Injury at 3T: Testing Inter- and Intramethodical Significance of ASL and DCE-MRI. PloS one. 2013;8(1):e53849.
69. Eikefjord E, Andersen E, Hodneland E, Zöllner F, Lundervold A, Svarstad E, et al. Use of 3D DCE-MRI for the Estimation of Renal Perfusion and Glomerular Filtration Rate: An Intrasubject Comparison of FLASH and KWIC With a Comprehensive Framework for Evaluation. American Journal of Roentgenology. 2015;204(3):W273-W81.
70. Wigh Lipso K, Hansen ESS, Tougaard RS, Laustsen C, Ardenkjaer-Larsen JH. Renal MR angiography and perfusion in the pig using hyperpolarized water. Magn Reson Med. 2017;78(3):1131-5.
71. Schrijvers BF, De Vriese AS, Flyvbjerg A. From hyperglycemia to diabetic kidney disease: the role of metabolic, hemodynamic, intracellular factors and growth factors/cytokines. Endocr Rev. 2004;25(6):971-1010.
72. Oates PJ. Aldose reductase inhibitors and diabetic kidney disease. Curr Opin Investig Drugs. 2010;11(4):402-17.
73. Grist JT, McLean MA, Riemer F, Schulte RF, Deen SS, Zaccagna F, et al. Quantifying normal human brain metabolism using hyperpolarized [1–13C]pyruvate and magnetic resonance imaging. NeuroImage. 2019;189:171-9.
74. Miloushev VZ, Granlund KL, Boltyanskiy R, Lyashchenko SK, DeAngelis LM, Mellinghoff IK, et al. Metabolic Imaging of the Human Brain with Hyperpolarized (13)C Pyruvate Demonstrates (13)C Lactate Production in Brain Tumor Patients. Cancer research. 2018;78(14):3755-60.
75. Aggarwal R, Vigneron DB, Kurhanewicz J. Hyperpolarized 1-[(13)C]-Pyruvate Magnetic Resonance Imaging Detects an Early Metabolic Response to Androgen Ablation Therapy in Prostate Cancer. European urology. 2017;72(6):1028-9.
76. Cunningham CH, Lau JY, Chen AP, Geraghty BJ, Perks WJ, Roifman I, et al. Hyperpolarized 13C Metabolic MRI of the Human Heart: Initial Experience. Circulation research. 2016;119(11):1177-82.
77. Nelson SJ, Kurhanewicz J, Vigneron DB, Larson PEZ, Harzstark AL, Ferrone M, et al. Metabolic Imaging of Patients with Prostate Cancer Using Hyperpolarized [1-13C]Pyruvate. Science Translational Medicine. 2013;5(198):198ra08.
78. Hato T, Friedman AN, Mang H, Plotkin Z, Dube S, Hutchins GD, et al. Novel application of complementary imaging techniques to examine in vivo glucose metabolism in the kidney. American journal of physiology Renal physiology. 2016;310(8):F717-f25.

79. Juillard L, Janier MF, Fouque D, Lionnet M, Le Bars D, Cinotti L, et al. Renal blood flow measurement by positron emission tomography using 15O-labeled water. Kidney international. 2000;57(6):2511-8.
80. Milshteyn E, von Morze C, Reed GD, Shang H, Shin PJ, Larson PEZ, et al. Using a local low rank plus sparse reconstruction to accelerate dynamic hyperpolarized (13)C imaging using the bSSFP sequence. J Magn Reson. 2018;290:46-59.
81. Durst M, Chiavazza E, Haase A, Aime S, Schwaiger M, Schulte RF. alpha-trideuteromethyl[15N]glutamine: A long-lived hyperpolarized perfusion marker. Magn Reson Med. 2016;76(6):1900-4.
82. Mariager CØ, Lindhardt J, Nielsen PM, Schulte RF, Ringgaard S, Laustsen C. Fractional Perfusion: A Simple Semi-Parametric Measure for Hyperpolarized 13C MR. IEEE Transactions on Radiation and Plasma Medical Sciences. 2019;3(4):523-7.
83. Lau JY, Chen AP, Gu YP, Cunningham CH. Voxel-by-voxel correlations of perfusion, substrate, and metabolite signals in dynamic hyperpolarized (13) C imaging. NMR in biomedicine. 2016;29(8):1038-47.